The Journal of the Astronautical Sciences, Vol. 55, No 3, July–September 2007, pp. 271–291

Analysis of Gravity-Gradient-Perturbed Rotational Dynamics at the Collinear Lagrange Points

Eytan Brucker[1] and Pini Gurfil[2]

Abstract

This paper studies the dynamics and stability of a rigid spacecraft subjected to gravity gradient torques exerted by the Sun and the Earth in the circular restricted three-body problem. We focus on the dynamics in a close vicinity to the Lagrangian collinear equilibrium points, and show that the linear stability domain predicted by the Beletskii-DeBra-Delp method in the two-body problem is modified due to the presence of an additional gravitating primary. The nonlinear differential equations are derived using a Hamiltonian formalism and are subsequently investigated using Poincaré maps. The effect of the gravity gradient torque is accentuated using difference Poincaré maps. The Melnikov integral method is utilized for studying the chaotic behavior of the gravity-gradient-perturbed system.

Introduction

The motion of a mass particle in a gravity field exerted by two massive bodies, the primaries, which rotate in circular orbits about their common barycenter, is known as the circular restricted three-body problem (RTBP). This dynamical system has five equilibrium points, known as the Lagrangian points. Three of these equilibria are collinear libration points, first found by Euler.

The RTBP has been thoroughly investigated since the late 1960s by Farquhar [1, 2], Hénon [3], Richardson [4], Gomez et al. [5], Barden and Howell [6], Papadakis [7], and Perdios [8]. These works studied several types of motions within the center manifold of the libration points in the circular RTBP. Three main types of periodic motion were detected: in-plane motion—horizontal Lyapunov orbits; out-of-plane motion—nearly vertical orbits; and halo orbits—resulting from a bifurcation of the Lyapunov orbits.

[1]Graduate Student, Faculty of Aerospace Engineering, Technion–Israel Institute of Technology, Haifa 32000, Israel.
[2]Senior Lecturer, Faculty of Aerospace Engineering, Technion–Israel Institute of Technology, Haifa 32000, Israel.

In the present study, we juxtapose the RTBP and another long-standing problem: the rotational dynamics of a rigid body. This problem has been studied by mathematicians, astronomers, and engineers over the past three centuries (cf. Gurfil et al. [9] and references therein).

Recently, there has been a renewed interest in obtaining analytical solutions for the perturbed rotational motion of an artificial satellite represented by the rigid-body approximation [10, 11, 12, 13, 14]. In particular, many efforts have been directed towards studying the effect of the gravity gradient (GG) torque on the rotational motion of a satellite in the dynamical setup of the two-body problem [15, 16, 10, 11, 17]. Since the effect of the GG torque decreases with altitude, a spacecraft located in the vicinity of the collinear Lagrangian points will be subjected to very small GG torques, exerted by both primaries. However, the subtle interaction between the two torques may offer some interesting dynamical features.

Barkin [18] and Kane [19] first derived solutions for some special cases of the said problem. Elipe [14] suggested to expand the GG perturbation into a Fourier series. Elipe's approach advocates approximating the solution since the GG torques render the rigid-body dynamics extremely difficult for an analytical solution—mainly because the usual Serret-Andoyer reduction procedure [9, 20] is not valid due to the presence of the Eulerian angles in the GG expressions. However, to the best of the authors' knowledge, thus far there has not been a dynamical-systems-based study of the nonlinear rotational dynamics of spacecraft perturbed by two GG-torques. It is this general perspective with which the current work is concerned.

The objective of this work is to examine how significant the influence of the GG torques is when considering the combined effect of the Sun and the Earth. The study focuses on the collinear Lagrange points and particularly on the L_2 point, as it is planned to host a number of future missions such as the James Webb Space Telescope and the multiple spacecraft of the Darwin project.

To gain an initial insight, we start with a linear analysis, used to determine new regions of stability in the Beletskii-DeBra-Delp sense [15, 16] vis-à-vis the two-body problem, and then extend it to the full, nonlinear, general problem. A set of differential equations modeling the rigid-body dynamics are derived based on a Hamiltonian formalism. A numerical method using the Poincaré section is then utilized to investigate the nonlinear equations of motion. The Poincaré section technique is used to trace differences between the torque-free equations of motion and the GG-perturbed equations. Finally, we use the Melnikov integral method [21] for identifying chaos.

The Gravity Gradient Torque

We first derive an expression for the GG torque acting on a vehicle in the circular RTBP setup by assuming that all the bodies are perfectly rigid (no tidal effects are considered).

Coordinate Systems

There are a few coordinate systems used in the subsequent discussion. The body frame, $\mathcal{B}$, is centered at the spacecraft's center of mass. The unit vectors, $\hat{\mathbf{i}}, \hat{\mathbf{j}}$, and $\hat{\mathbf{k}} = \hat{\mathbf{i}} \times \hat{\mathbf{j}}$ coincide with the principal axes as shown in Fig. 1. The frame $\mathcal{B}$, as all the other frames in this work, is a Cartesian, rectangular, dextral frame. The orbital frame, $\mathcal{L}$, is also centered at the body center of mass, oriented such that its third unit vector, $\hat{\mathbf{R}}$, is directed towards the barycenter; $\hat{\mathbf{j}}_{\mathcal{L}}$ is perpendicular to the plane of

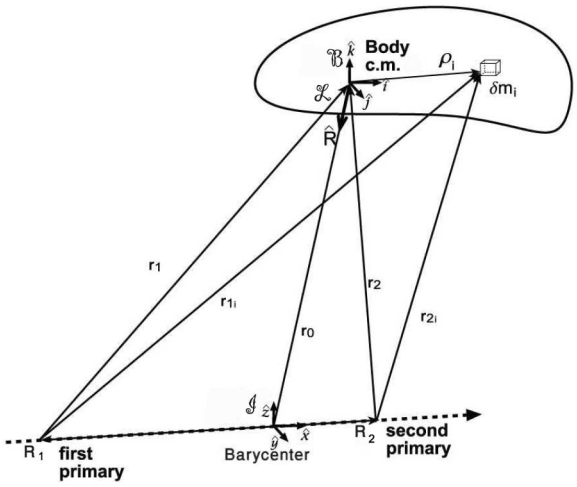

FIG. 1. A rigid spacecraft is subjected to a gravity gradient torque in the restricted three-body problem. The three reference frames used to describe the motion are the body frame, the orbital frame, and the inertial frame [22].

motion and $\hat{\mathbf{i}}_{\mathcal{L}}$ completes the triad. The inertial frame, $\mathcal{I}$, is centered at the barycenter, and is defined by the unit vector $\hat{\mathbf{x}}$, directed towards the initial position of the second primary; $\hat{\mathbf{z}}$, which is perpendicular to the motion plane; and $\hat{\mathbf{y}}$, which completes the setup, as shown in Fig. 1.

The Gravity Gradient Torque in the Restricted Three-Body Problem

The GG torque, $\mathbf{T}_G$, acting on a mass element, $\mathrm{d}m_i$, located at $\boldsymbol{\rho}_i$ in frame $\mathcal{B}$, due to the presence of a gravitational force, $\mathbf{F}_i$ (assuming a uniform mass distribution), is given by

$$\mathbf{T}_G = \int \boldsymbol{\rho}_i \times \mathrm{d}\mathbf{F}_i \tag{1}$$

We now define the following notation: μ_1 and μ_2 are the gravitational constants of the primaries, $\mathbf{R}_1$ and $\mathbf{R}_2$ are the position vectors of the primaries in the barycentric frame, $\mathbf{r}_{1_i}$ and $\mathbf{r}_{2_i}$ are the positions vectors of the mass element with respect to the primaries, and $\mathbf{r}_0$ is the position vector of the spacecraft's center of mass relative to the barycenter, as shown in Fig. 1. Since

$$\mathrm{d}\mathbf{F}_i = \left[-\frac{\mu_1}{|\mathbf{r}_{1_i}|^3}\,\mathbf{r}_{1_i} - \frac{\mu_2}{|\mathbf{r}_{2_i}|^3}\,\mathbf{r}_{2_i} \right] \mathrm{d}m_i \tag{2}$$

then

$$\begin{aligned} \mathbf{T}_G &= \int \boldsymbol{\rho}_i \times \left[-\frac{\mu_1}{|\mathbf{r}_{1_i}|^3}\,\mathbf{r}_{1_i} - \frac{\mu_2}{|\mathbf{r}_{2_i}|^3}\,\mathbf{r}_{2_i} \right] \mathrm{d}m_i \\ &= -\int \boldsymbol{\rho}_i \times \left[\frac{\mu_1}{|\mathbf{r}_0 - \mathbf{R}_1 + \boldsymbol{\rho}_i|^3}[\mathbf{r}_0 - \mathbf{R}_1 + \boldsymbol{\rho}_i] \right. \\ &\quad \left. + \frac{\mu_2}{|\mathbf{r}_0 - \mathbf{R}_2 + \boldsymbol{\rho}_i|^3}[\mathbf{r}_0 - \mathbf{R}_2 + \boldsymbol{\rho}_i] \right] \mathrm{d}m_i \end{aligned} \tag{3}$$

As shown in Fig. 1, we can define $\mathbf{r}_1 = \mathbf{r}_0 - \mathbf{R}_1$ and $\mathbf{r}_2 = \mathbf{r}_0 - \mathbf{R}_2$, yielding

$$\mathbf{T}_G = -\int \boldsymbol{\rho}_i \times \left[\frac{\mu_1}{|\mathbf{r}_1 + \boldsymbol{\rho}_i|^3}[\mathbf{r}_1 + \boldsymbol{\rho}_i] + \frac{\mu_2}{|\mathbf{r}_2 + \boldsymbol{\rho}_i|^3}[\mathbf{r}_2 + \boldsymbol{\rho}_i] \right] \mathrm{d}m_i$$

Assuming that $\boldsymbol{\rho}_i \lll \mathbf{r}_1, \mathbf{r}_2$, a binomial approximation gives

$$\begin{aligned}\mathbf{T}_G &\approx -\int \boldsymbol{\rho}_i \times \left\{ \frac{\mu_1}{r_1^3}[\mathbf{r}_1 + \boldsymbol{\rho}_i]\left[1 - 3\frac{\mathbf{r}_1\boldsymbol{\rho}_i}{r_1^2}\right] + \frac{\mu_2}{r_2^3}[\mathbf{r}_2 + \boldsymbol{\rho}_i]\left[1 - 3\frac{\mathbf{r}_2\boldsymbol{\rho}_i}{r_2^2}\right] \right\} \mathrm{d}m_i \\ &= -\frac{\mu_1}{r_1^3}\int \boldsymbol{\rho}_i \times \mathbf{r}_1\left[1 - 3\frac{\mathbf{r}_1\boldsymbol{\rho}_i}{r_1^2}\right]\mathrm{d}m_i + \frac{\mu_2}{r_2^3}\int \boldsymbol{\rho}_i \times \mathbf{r}_2\left[1 - 3\frac{\mathbf{r}_2\boldsymbol{\rho}_i}{r_2^2}\right]\mathrm{d}m_i\end{aligned}$$

Due to the fact that the coordinate system is located at the center of mass

$$\mathbf{T}_G \approx 3\frac{\mu_1}{r_1^5}\int \mathbf{r}_1(\boldsymbol{\rho}_i \cdot \boldsymbol{\rho}_i) \times \mathbf{r}_1\,\mathrm{d}m_i + 3\frac{\mu_2}{r_2^5}\int \mathbf{r}_2(\boldsymbol{\rho}_i \cdot \boldsymbol{\rho}_i) \times \mathbf{r}_2\,\mathrm{d}m_i$$

Defining the inertia tensor as $\mathbb{I} = \int_m (\rho^2 I - \boldsymbol{\rho} \cdot \boldsymbol{\rho})\mathrm{d}m$ yields

$$\mathbf{r}_k\mathbb{I} \times \mathbf{r}_k = \int [\mathbf{r}_k(\rho^2 I) \times \mathbf{r}_k - \mathbf{r}_k(\boldsymbol{\rho} \cdot \boldsymbol{\rho}) \times \mathbf{r}_k]\mathrm{d}m \tag{4}$$

where I is the identity matrix and $k = 1, 2$, so that

$$\begin{aligned}T_G &\approx -3\frac{\mu_1}{r_1^5}\mathbb{I}\mathbf{r}_1 \times \mathbf{r}_1 - 3\frac{\mu_2}{r_2^5}\mathbb{I}\mathbf{r}_2 \times \mathbf{r}_2 \\ &= 3\frac{\mu_1}{r_1^5}\mathbf{r}_1 \times \mathbb{I}\mathbf{r}_1 + 3\frac{\mu_2}{r_2^5}\mathbf{r}_2 \times \mathbb{I}\mathbf{r}_2 \\ &= 3\frac{\mu_1}{r_1^3}\hat{\mathbf{r}}_1 \times \mathbb{I}\hat{\mathbf{r}}_1 + 3\frac{\mu_2}{r_2^3}\hat{\mathbf{r}}_2 \times \mathbb{I}\hat{\mathbf{r}}_2\end{aligned} \tag{5}$$

Thus, the gravitational torque exerted by two primaries (the Sun and the Earth in our subsequent quantitative analysis) on a spacecraft is given by

$$\mathbf{T}_G \approx 3\frac{\mu_1}{r_1^3}\hat{\mathbf{r}}_1 \times \mathbb{I}\hat{\mathbf{r}}_1 + 3\frac{\mu_2}{r_2^3}\hat{\mathbf{r}}_2 \times \mathbb{I}\hat{\mathbf{r}}_2 \tag{6}$$

Assuming that the spacecraft is fixed to one of the Lagrange collinear libration points, it will orbit the barycenter in a circular orbit together with the primaries, moving in a constant angular velocity. Moreover, if the spacecraft is fixed to L_2, then the unit vectors $\hat{\mathbf{r}}_1$ and $\hat{\mathbf{r}}_2$, directed from the spacecraft's center of mass to the primaries, will coincide with the unit vector $\hat{\mathbf{R}}$. Thus, (6) will become

$$\mathbf{T}_G = -\frac{3\mu_1}{r_1^3}\mathbb{I}\hat{\mathbf{R}} \times \hat{\mathbf{R}} - \frac{3\mu_2}{r_2^3}\mathbb{I}\hat{\mathbf{R}} \times \hat{\mathbf{R}} \tag{7}$$

Linear Analysis

The Linear Equations of Motion

Let us write the transformation matrix, A, which transforms from the orbital frame to the body frame assuming small angles [22]. In the linear approximation, the rotation sequence is not important, and the resulting matrix is

$$A = \begin{pmatrix} 1 & \psi & -\theta \\ -\psi & 1 & \phi \\ \theta & -\phi & 1 \end{pmatrix} \tag{8}$$

where ψ, ϕ, and θ are the Euler angles. In order to express $\hat{\mathbf{R}}$ in the body frame, we can use the relationship

$$[\hat{\mathbf{R}}]_{\mathcal{B}} = A[\hat{\mathbf{R}}]_{\mathcal{L}} = A\begin{pmatrix} 0 \\ 0 \\ -1 \end{pmatrix} = \begin{pmatrix} \theta \\ -\phi \\ -1 \end{pmatrix} \tag{9}$$

Let us define

$$n_1^2 = \frac{\mu_1}{r_1^3}, \qquad n_2^2 = \frac{\mu_2}{r_2^3} \tag{10}$$

Substituting $\hat{\mathbf{R}}$ into equation (7) and using the small angles assumption gives

$$\mathbf{T}_G = [-3\phi(I_2 - I_3)(n_1^2 + n_2^2)]\hat{\mathbf{i}} + [3\theta(I_3 - I_1)(n_1^2 + n_2^2)]\hat{\mathbf{j}} \tag{11}$$

where I_1, I_2, and I_3 are the moments of inertia in principal axes. The expression for $\mathbf{T}_G$ is now substituted into Euler's equations to give

$$\mathbf{T}_G = \frac{\mathrm{d}\mathbf{H}}{\mathrm{d}t} + \boldsymbol{\omega} \times \mathbf{H} \tag{12}$$

where $\boldsymbol{\omega}$ is the body angular velocity vector and $\mathbf{H}$ is the angular momentum vector. We now use the relationships

$$\mathbf{H} = \mathbb{I}\boldsymbol{\omega} \tag{13}$$

and

$$(\boldsymbol{\omega}_{\mathcal{B}/\mathcal{I}})_{\mathcal{B}} = (\boldsymbol{\omega}_{\mathcal{B}/\mathcal{L}})_{\mathcal{B}} + (\boldsymbol{\omega}_{\mathcal{L}/\mathcal{I}})_{\mathcal{B}} \tag{14}$$

where the $\mathcal{B}/\mathcal{I}$, $\mathcal{B}/\mathcal{L}$, and $\mathcal{L}/\mathcal{I}$ indices refer to the angular velocity of the body frame with respect to the inertial frame, the body frame with respect to the orbital frame, and the orbit frame with respect to the inertial frame, respectively. Substitution entails

$$\boldsymbol{\omega} = \begin{pmatrix} \dot{\phi} \\ \dot{\theta} \\ \dot{\psi} \end{pmatrix} + A\begin{pmatrix} 0 \\ -n_0 \\ 0 \end{pmatrix} \tag{15}$$

where n_0 denotes the constant angular velocity of the system, given by

$$n_0 = \sqrt{\frac{\mu_1 + \mu_2}{r_0^3}} \tag{16}$$

Substituting equations (13)–(15) into (12), assuming that the moments of inertia are aligned with the principal axes, and neglecting products of small quantities gives

$$\begin{aligned} \frac{\mathrm{d}\mathbf{H}}{\mathrm{d}t} + \boldsymbol{\omega} \times \mathbf{H} &= \mathbb{I}\frac{\mathrm{d}\boldsymbol{\omega}}{\mathrm{d}t} + \boldsymbol{\omega} \times \mathbb{I}\boldsymbol{\omega} \\ &= [I_1(\ddot{\phi} - n_0\dot{\psi}) - n_0\dot{\psi}(I_3 - I_2) - n_0^2\phi(I_3 - I_2)]\hat{\mathbf{i}} \\ &\quad + I_2\ddot{\theta}\hat{\mathbf{j}} + [I_3(\ddot{\psi} + n_0\dot{\phi}) - n_0\dot{\phi}(I_2 - I_1) + n_0^2\psi(I_2 - I_1)]\hat{\mathbf{k}} \end{aligned} \tag{17}$$

Substituting (17) and (11) into (12) leads to the linear equations

$$\ddot{\phi} = -\sigma_x(n_0^2 + 3n_1^2 + 3n_2^2)\phi + (1 - \sigma_x)n_0\dot{\psi} \tag{18}$$

$$\ddot{\theta} = -3\sigma_y(n_1^2 + n_2^2)\theta \tag{19}$$

$$\ddot{\psi} = -\sigma_z n_0^2\psi - (1 - \sigma_z)n_0\dot{\phi} \tag{20}$$

where σ_x, σ_y, and σ_z are defined as

$$\sigma_x = \left(\frac{I_2 - I_3}{I_1}\right) \tag{21}$$

$$\sigma_y = \left(\frac{I_1 - I_3}{I_2}\right) \tag{22}$$

$$\sigma_z = \left(\frac{I_2 - I_1}{I_3}\right) \tag{23}$$

and their values are bounded by $|\sigma_{x,y,z}| < 1$.

Note that the pitch channel, equation (19), is decoupled from roll (18) and yaw (20), similarly to the two-body problem.

Stability Analysis

For stability in pitch it is required that $\sigma_y > 0$. In order to determine the stability of the roll and yaw dynamics, one should find the roots of the characteristic polynomial generated by equations (18) and (20)

$$\Delta = s^4 + \Lambda_1 n_0^2 s^2 + n_0^4 \Lambda_2 \sigma_x \sigma_z \tag{24}$$

where

$$\Lambda_1 = 1 + \sigma_x\sigma_z + 3\sigma_x\left[\left(\frac{n_1}{n_0}\right)^2 + \left(\frac{n_2}{n_0}\right)^2\right] \tag{25}$$

$$\Lambda_2 = 3\left(\frac{n_1}{n_0}\right)^2 + 3\left(\frac{n_2}{n_0}\right)^2 + 1 \tag{26}$$

Calculating the constants n_0, n_1, and n_2 for the L_2 point in the Sun-Earth system yields $(n_1/n_0)^2 = 0.97$ and $(n_2/n_0)^2 = 3$, which gives

$$\Delta = s^4 + [1 + 11.91\sigma_x + \sigma_x\sigma_z]n_0^2 s^2 + 12.91 n_0^4 \sigma_x\sigma_z \tag{27}$$

Requiring that Δ be a Hurwitz polynomial gives the inequality

$$1 + 11.91\sigma_x + \sigma_x\sigma_z > 2\sqrt{12.91\sigma_x\sigma_z} \tag{28}$$

Requiring positive coefficient for Δ gives the conditions for stability as

$$1 + 11.91\sigma_x + \sigma_x\sigma_z > 0$$
$$\sigma_x\sigma_z > 0$$

The necessary and sufficient conditions for linear stability are then

$$\sigma_y > 0$$
$$1 + 11.91\sigma_x + \sigma_x\sigma_z > 2\sqrt{12.91\sigma_x\sigma_z} \tag{29}$$
$$\sigma_x\sigma_z > 0$$

The stability conditions for the two-body problem depend on the moments of inertia only. In the three-body case the situation is different, as (24) implies. In general, the satellite's attitude will remain stable if the centrifugal torques balance the gravitational torques. In the classical, two-body case, this occurs in two regions. One region is the Lagrange pitch stability region, which is decoupled from yaw and roll, and the other is the Beletskii-DeBra-Delp region. These regions are determined by the satellite's geometry only, as implied by the roll-yaw Beletskii-DeBra-Delp stability limit of the two-body problem [15, 16]

$$1 + 3\sigma_x + \sigma_x\sigma_z > 4\sqrt{\sigma_x\sigma_z} \tag{30}$$

Systems with more than one primary have another factor which affects the roll-yaw inequality and the Beletskii-DeBra-Delp stability region. This factor is [26]

$$\left(\frac{n_1}{n_0}\right)^2 + \left(\frac{n_2}{n_0}\right)^2 \tag{31}$$

Figure 2 shows the resulting regions of stability in two different cases: the well-known stability region of the two-body problem, and the same stability region generalized to the RTBP. The stability regions in the RTBP are composed from the Lagrange pitch stability condition, which is similar to the two-body case, and equation (28), the modified Beletskii-DeBra-Delp region, which has been reduced compared to the two-body case.

The Nonlinear Equations of Motion

In order to derive the general equations of motion, we derive the Hamiltonian for our dynamical system. This Hamiltonian will be formulated by using Euler

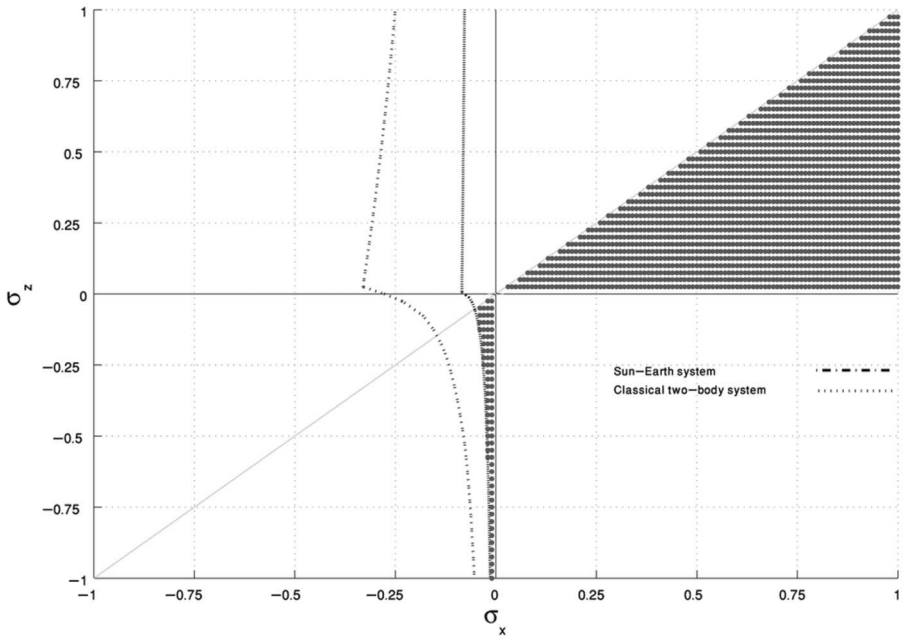

FIG. 2. Comparison of Beletskii-DeBra-Delp stability regions between the two-body and restricted three-body problems. The spacecraft is located at L_2 in the Sun-Earth system. The shaded regions represent stable motion.

angles as generalized coordinates. The general expression for the Hamiltonian is written as

$$\mathcal{H} = \mathcal{H}_0 + \mathcal{H}_G \tag{32}$$

where $\mathcal{H}_0$ represents the Hamiltonian of the free-spin, and $\mathcal{H}_G$ is the Hamiltonian resulting from the GG torques applied by the primaries.

The Free-Spin Hamiltonian

To get the first part of the Hamiltonian, $\mathcal{H}_0$, we assume free rotational motion and use the Legendre transformation

$$\mathcal{H}_0 = \sum_{i=1}^{3} \dot{q}_i p_i - \mathcal{L} \tag{33}$$

where $\mathcal{L}$ is the Lagrangian, q_i is a generalized coordinate, $q_1 = \phi$, $q_2 = \theta$, $q_3 = \psi$, and p_i is a conjugate momenta, $p_1 = \Phi$, $p_2 = \Theta$, $p_3 = \Psi$. $\mathcal{H}_0$ is thus given by

$$\mathcal{H}_0 = \dot{\phi}\Phi + \dot{\theta}\Theta + \dot{\psi}\Psi - \mathcal{L} \tag{34}$$

The Lagrangian equals the rotational kinetic energy

$$\mathcal{L} = \frac{1}{2}\,\boldsymbol{\omega}\mathbb{I}\boldsymbol{\omega} \tag{35}$$

The p_i are calculated by

$$p_i = \frac{\partial \mathcal{L}}{\partial \dot{q}_i} \tag{36}$$

Thus

$$\Phi = \frac{\partial \mathcal{L}}{\partial \dot{\phi}}; \qquad \Theta = \frac{\partial \mathcal{L}}{\partial \dot{\theta}}; \qquad \Psi = \frac{\partial \mathcal{L}}{\partial \dot{\psi}} \tag{37}$$

Evaluating equation (34) gives

$$\begin{aligned}\mathcal{H}_0 = {} & \frac{1}{2}\left(\frac{\sin^2\psi}{I_1} + \frac{\cos^2\psi}{I_2}\right)\left(\frac{\Phi - \Psi\cos\theta}{\sin\theta}\right)^2 \\ & + \frac{1}{2}\left(\frac{\cos^2\psi}{I_1} + \frac{\sin^2\psi}{I_2}\right)\Theta^2 + \frac{1}{2}\left(\frac{1}{I_1} - \frac{1}{I_2}\right)\left(\frac{\Phi - \Psi\cos\theta}{\sin\theta}\right)\Theta\sin\psi\cos\psi \\ & + \frac{\Psi^2}{2I_3}\end{aligned} \tag{38}$$

The Perturbing Hamiltonian

The second part of the Hamiltonian, $\mathcal{H}_G$, comprises the potentials of both perturbing gravitational torques

$$\mathcal{H}_G = \mathcal{H}_{G_1} + \mathcal{H}_{G_2} \tag{39}$$

where $\mathcal{H}_{G_1}$ and $\mathcal{H}_{G_2}$ are the Hamiltonians due to the GG torques of the first and second primary, respectively.

The GG torque potential of the first primary can be calculated as

$$\begin{aligned} V &= -\int \frac{\mu_1}{\mathbf{r}_{1_i}}\,\mathrm{d}m_1 \\ &= -\int \frac{\mu_1}{\mathbf{r}_1+\boldsymbol{\rho}_i}\,\mathrm{d}m_1 \\ &= -\int \frac{\mu_1}{r_1}\left[1+2\frac{\boldsymbol{\rho}_i}{r_1}\cdot\frac{\mathbf{r}_1}{r_1}+\left(\frac{\rho_i}{r_1}\right)^2+\mathcal{O}\left(\frac{\rho_i^3}{r_1^3}\right)\right]^{-\frac{1}{2}}\mathrm{d}m_1 \end{aligned} \tag{40}$$

Since $\boldsymbol{\rho}_i \lll \mathbf{r}_1$, we can expand equation (40) into a Legendre series using Legendre polynomials up to second-order terms in $\boldsymbol{\rho}_i$. This procedure entails

$$V = -\frac{\mu_1}{r_1}\int\left\{1-\frac{\boldsymbol{\rho}_i}{r_1}\cdot\frac{\mathbf{r}_1}{r_1}+\frac{1}{2}\left[3\left(\frac{\mathbf{r}_1}{r_1}\right)^2-1\right]\left(\frac{\boldsymbol{\rho}_i}{r_1}\right)^2\right\}\mathrm{d}m_1 \tag{41}$$

$$= -\frac{\mu_1}{r_1}m_1\frac{\mu_1}{r_1^2}\int\underbrace{\frac{\mathbf{r}_1\cdot\boldsymbol{\rho}_i}{r_1}}_{=0}\mathrm{d}m_1-\frac{\mu_1}{2r_1^3}\int 3\left(\frac{\mathbf{r}_1\cdot\boldsymbol{\rho}_i}{r_1}\right)^2\mathrm{d}m_1$$

$$+\frac{\mu_1}{2r_1^3}\int\boldsymbol{\rho}_i^2\,\mathrm{d}m_1 \tag{42}$$

The second term in equation (42) has been eliminated due to the fact that the body frame is centered at the center of mass.

Using the inertia tensor definition and transforming it into principal axes yields the form known as the MacCullagh formula [23]

$$V = -\frac{\mu_1}{r_1}m_1+\frac{3}{2}\frac{\mu_1}{r_1^3}(I_1\alpha_1^2+I_2\beta_1^2+I_3\gamma_1^2)-\frac{\mu_1}{2r_1^3}\,\mathrm{trace}(\mathbb{I})$$

where α_1, β_1, and γ_1 are the direction cosines, to be defined shortly. Utilizing the identity

$$\alpha_1^2+\beta_1^2+\gamma_1^2=1 \tag{43}$$

yields

$$V = -\frac{\mu_1}{r_1}m_1+\frac{3}{2}\frac{\mu_1}{r_1^3}[(I_2-I_1)\beta_1^2+(I_3-I_1)\gamma_1^2]+\frac{\mu_1}{2r_1^3}(I_1-I_2-I_3) \tag{44}$$

The perturbing Hamiltonian due to the GG torque applied by the first primary equals the second term of the potential (44)

$$\mathcal{H}_{G_1} = \frac{3}{2}\frac{\mu_1}{r_1^3}[(I_2-I_1)\beta_1^2+(I_3-I_1)\gamma_1^2] \tag{45}$$

We could use all three terms, that is, take $\mathcal{H}_{G_1}=V$. However, the terms that are not orientation-depended will be eliminated while deriving the system's equations of motion.

The expression for $\mathcal{H}_{G_2}$ can be evaluated similarly to $\mathcal{H}_{G_1}$, so based on equation (39) we get

$$\mathcal{H}_G = \frac{3}{2}\frac{\mu_1}{r_1^3}[(I_2 - I_1)\beta_1^2 + (I_3 - I_1)\gamma_1^2] + \frac{3}{2}\frac{\mu_2}{r_2^3}[(I_2 - I_1)\beta_2^2 + (I_3 - I_1)\gamma_2^2] \quad (46)$$

Rearranging (46) yields

$$\mathcal{H}_G = \frac{3}{2}\left[(I_2 - I_1)\left(\frac{\mu_1}{r_1^3}\beta_1^2 + \frac{\mu_2}{r_2^3}\beta_2^2\right) + (I_3 - I_1)\left(\frac{\mu_1}{r_1^3}\gamma_1^2 + \frac{\mu_2}{r_2^3}\gamma_2^2\right)\right] \quad (47)$$

We now use the definition for the direction cosines as

$$\beta_1 = \hat{\mathbf{j}} \cdot \hat{\mathbf{r}}_1 \qquad \gamma_1 = \hat{\mathbf{k}} \cdot \hat{\mathbf{r}}_1 \quad (48)$$

$$\beta_2 = \hat{\mathbf{j}} \cdot \hat{\mathbf{r}}_2 \qquad \gamma_2 = \hat{\mathbf{k}} \cdot \hat{\mathbf{r}}_2 \quad (49)$$

where $\hat{\mathbf{r}}_1$ and $\hat{\mathbf{r}}_2$ are inertial unit vectors and $\hat{\mathbf{j}}$ and $\hat{\mathbf{k}}$ are unit vectors along the body principal axes. The rotation matrix from the inertial to the body frame, obtained by using the 3-1-3 rotation sequence, is given by

$$\tilde{A} = \begin{pmatrix} c_\psi c_\phi - s_\psi c_\theta s_\phi & -c_\psi s_\phi - s_\psi c_\theta c_\phi & s_\phi s_\theta \\ s_\psi c_\phi - c_\psi c_\theta s_\phi & -s_\psi s_\phi + c_\psi c_\theta c_\phi & -c_\psi s_\theta \\ s_\theta s_\phi & s_\theta c_\phi & c_\theta \end{pmatrix} \quad (50)$$

where we have used the shortened notation $c_{(\cdot)} = \cos(\,\cdot\,)$, $s_{(\cdot)} = \sin(\,\cdot\,)$. To transform the body principal axes into an inertial frame, we write

$$\hat{\mathbf{y}} = \tilde{A}\hat{\mathbf{j}}, \qquad \hat{\mathbf{z}} = \tilde{A}\hat{\mathbf{k}} \quad (51)$$

$$\hat{\mathbf{j}} = \begin{pmatrix} 0 \\ 1 \\ 0 \end{pmatrix}, \qquad \hat{\mathbf{k}} = \begin{pmatrix} 0 \\ 0 \\ 1 \end{pmatrix} \quad (52)$$

The inertial unit vectors are given by

$$\hat{\mathbf{r}}_1 = \left[\frac{x - R_1}{|\mathbf{r}_1|}, \frac{y}{|\mathbf{r}_1|}, \frac{z}{|\mathbf{r}_1|}\right]$$

$$\hat{\mathbf{r}}_2 = \left[\frac{x - R_2}{|\mathbf{r}_2|}, \frac{y}{|\mathbf{r}_2|}, \frac{z}{|\mathbf{r}_2|}\right] \quad (53)$$

where

$$|\mathbf{r}_1| = \sqrt{(x - R_1)^2 + y^2 + z^2}, \qquad |\mathbf{r}_2| = \sqrt{(x - R_2)^2 + y^2 + z^2} \quad (54)$$

(x, y, z) denote the local position of the spacecraft in the orbit rotating frame, and R_1 and R_2 are the primaries' distances from the common barycenter. As shown in Fig. 3, while pointing to one of the collinear Lagrange points, the vectors $\mathbf{r}_0$, $\mathbf{r}_1$, and $\mathbf{r}_2$ become parallel; thus, while pointing to L_2 these vectors are parallel and are pointing to the same direction.

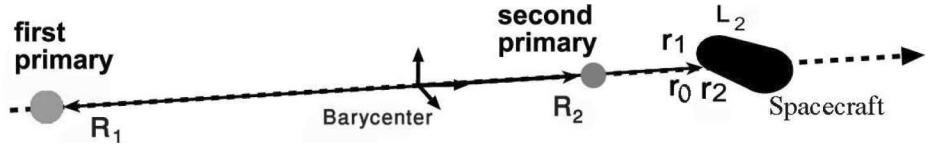

FIG. 3. A Spacecraft Fixed to L_2 Simplifies the Hamiltonian Formulation of the Equations of Motion.

Now, suppose that the spacecraft mean orbit radius around one of the libration points is small compared to the distance from the primaries to the selected libration point, so it can be neglected. Under this assumption, the spacecraft is fixed (geometrically) to the libration point—say L_2. This situation is illustrated by Fig. 3. The mathematical formulation of this assumption can be written by substituting the following relationships into equation (54): $x - R_1 = |\mathbf{r}_1|$, $x - R_2 = |\mathbf{r}_2|$ and $y = z = 0$. This leads to

$$\hat{\mathbf{r}}_0 = \hat{\mathbf{r}}_1 = \hat{\mathbf{r}}_2 = \begin{pmatrix} 1 \\ 0 \\ 0 \end{pmatrix} \tag{55}$$

The direction cosines assume the form

$$\beta_1 = \beta_2 = \beta, \qquad \gamma_1 = \gamma_2 = \gamma \tag{56}$$

and $\mathcal{H}_G$ reduces to

$$\mathcal{H}_G = \frac{3}{2}\left[\beta^2(I_2 - I_1)\left(\frac{\mu_1}{r_1^3} + \frac{\mu_2}{r_2^3}\right) + \gamma^2(I_3 - I_1)\left(\frac{\mu_1}{r_1^3} + \frac{\mu_2}{r_2^3}\right)\right] \tag{57}$$

where

$$\beta = -c_\psi s_\phi - s_\psi c_\theta c_\phi, \qquad \gamma = s_\phi s_\theta \tag{58}$$

The Nonlinear Equations of Motion

Hamilton's equations are

$$\dot{\Phi} = -\frac{\partial \mathcal{H}_0}{\partial \phi} - \frac{\partial \mathcal{H}_G}{\partial \phi} \tag{59a}$$

$$\dot{\Theta} = -\frac{\partial \mathcal{H}_0}{\partial \theta} - \frac{\partial \mathcal{H}_G}{\partial \theta} \tag{59b}$$

$$\dot{\Psi} = -\frac{\partial \mathcal{H}_0}{\partial \psi} - \frac{\partial \mathcal{H}_G}{\partial \psi} \tag{59c}$$

$$\dot{\phi} = \frac{\partial \mathcal{H}_0}{\partial \Phi} + \frac{\partial \mathcal{H}_G}{\partial \Phi} \tag{59d}$$

$$\dot{\theta} = \frac{\partial \mathcal{H}_0}{\partial \Theta} + \frac{\partial \mathcal{H}_G}{\partial \Theta} \tag{59e}$$

$$\dot{\psi} = \frac{\partial \mathcal{H}_0}{\partial \Psi} + \frac{\partial \mathcal{H}_G}{\partial \Psi} \tag{59f}$$

We can now obtain the full differential equations by substituting equations (38) and (57) into equations (59)

$$\dot{\Phi} = -2k_1(c_\psi s_\phi + s_\psi c_\theta c_\phi)(c_\psi c_\phi - s_\psi c_\theta s_\phi)(k_3 + k_4) \tag{60a}$$

$$\begin{aligned}\dot{\Theta} = {} & (-\Phi c_\theta + \Psi c_\theta^2 + \Psi s_\theta^2) \\ & \times \frac{\Psi c_\theta s_\psi^2 I_2 + \Psi c_\theta c_\psi^2 I_1 - s_\psi^2 I_2 \Phi - \Theta s_\psi c_\psi s_\theta I_2 + \Theta s_\psi c_\psi s_\theta I_1 - c_\psi^2 I_1 \Phi}{I_1 I_2 s_\theta^3} \\ & + 2k_1 s_\psi s_\theta (k_3 + k_4)(c_\phi c_\psi s_\phi + s_\psi c_\phi^2 c_\theta - c_\theta s_\psi k_2)\end{aligned} \tag{60b}$$

$$\dot{\Psi} = (I_2 - I_1)(-c_\psi \Phi + \Psi c_\theta c_\psi + s_\psi \Theta s_\theta)\frac{s_\psi \Phi - s_\psi c_\theta \Psi + \Theta c_\psi s_\theta}{I_1 I_2 s_\theta^2}$$
$$- 2k_1(k_3 + k_4)(c_\psi^2 s_\phi c_\theta c_\phi - s_\psi^2 c_\theta c_\phi s_\phi + s_\psi c_\theta^2 c_\phi^2 c_\psi - c_\psi s_\phi^2 s_\psi$$
$$+ k_2 s_\psi s_\theta^2 c_\psi) \tag{60c}$$

$$\dot{\phi} = \left(\frac{1}{I_1}s_\psi^2 + \frac{1}{I_2}c_\psi^2\right)\frac{\Phi - \Psi c_\theta}{s_\theta^2} + \left(\frac{1}{I_1} - \frac{1}{I_2}\right)\frac{\Theta s_\psi c_\psi}{s_\theta} \tag{60d}$$

$$\dot{\theta} = \left(\frac{1}{I_1}c_\psi^2 + \frac{1}{I_2}s_\psi^2\right)\Theta + \left(\frac{1}{I_1} - \frac{1}{I_2}\right)\frac{(\Phi - \Psi c_\theta)s_\psi c_\psi}{s_\theta} \tag{60e}$$

$$\dot{\psi} = -\left(\frac{1}{I_1}s_\psi^2 + \frac{1}{I_2}c_\psi^2\right)\frac{\Phi - \Psi c_\theta}{s_\theta^2}c_\theta - \left(\frac{1}{I_1} - \frac{1}{I_2}\right)\frac{c_\theta \Theta s_\psi c_\psi}{s_\theta} + \frac{\Psi}{I_3} \tag{60f}$$

where

$$k_1 = \frac{3}{2}(I_2 - I_1); \qquad k_2 = \frac{I_2 - I_1}{I_3 - I_1}; \qquad k_3 = \frac{\mu_1}{r_1^3}; \qquad k_4 = \frac{\mu_2}{r_2^3} \tag{61}$$

A more compact form of equations (60d)–(60f) can be written as

$$\dot{\phi} = \frac{I_1 c_\psi g_2 + I_2 s_\psi g_1}{I_1 I_2 s_\theta} \tag{62a}$$

$$\dot{\theta} = \frac{I_2 c_\psi g_1 - I_1 s_\psi g_2}{I_1 I_2} \tag{62b}$$

$$\dot{\psi} = -\frac{I_1 I_3 c_\psi c_\theta g_2 + I_3 I_2 s_\psi c_\theta g_1 - I_1 I_2 g_3 s_\theta}{I_1 I_2 I_3 s_\theta} \tag{62c}$$

where g_1, g_2, g_3 are the components of angular momentum in the body frame [9]

$$g_1 = \frac{\Phi - \Psi c_\theta}{s_\theta}s_\psi + \Theta c_\psi \tag{63a}$$

$$g_2 = \frac{\Phi - \Psi c_\theta}{s_\theta}c_\psi + \Theta s_\psi \tag{63b}$$

$$g_3 = \Psi \tag{63c}$$

Poincaré Maps

The Method

Poincaré maps are useful for studying nearly periodic motion. With Poincaré maps, one can quantitatively determine chaotic regions, and inquire how the chaotic behavior of the motion evolves from one set of initial conditions to another [24, 25]. A Poincaré map is a cross-section of the phase-space generated by the system flow. In general, the maps are created by determining a value for the Hamiltonian, setting the initial conditions for the reduced system, and choosing a Poincaré surface of section. By doing so, the problem reduces into two degrees of freedom. Broucke [17] first applied the Poincaré method for studying the phase space of perturbed attitude dynamics in the two-body problem. Broucke's work did not study the GG-perturbed attitude dynamics, but rather the rotational dynamics induced by a misalignment between the center of mass and the center of gravity.

Using Poincaré maps in order to generate Poincaré sections could be helpful when it is difficult to qualitatively study the dynamical system based on its phase space only, and when the perturbation affecting the system is relatively small in comparison to the unperturbed dynamics. In the present problem, both of these features exist. We will therefore use the the Poincaré section method in order to study the nonlinear problem.

An important caveat is that during the numerical integration of equations (60), performed using an eighth-order Runge-Kutta integrator, the Hamiltonian might not remain constant due to numerical errors arising from the dissipative nature of the Runge-Kutta algorithm. These errors cause secular growth in the state variables. In order to mitigate this effect, the least squares method was used to "symplify" the Runge-Kutta integrator in each time step, thus yielding a constant Hamiltonian.

Numerical Results

The Poincaré maps were generated for a spacecraft stationed at the Sun-Earth L_2 point with $\mathcal{H} = 50\ \mathrm{N} \cdot \mathrm{m}$ at the section $\theta = 3\pi/2$. The initial conditions were $\phi_0 = 0.05$ rad and $\Phi_0 = 10\ \mathrm{kg\ m^2/sec}$. The additional initial conditions were chosen as follows. We distinguish between two cases, each having different moments of inertia. For Case I,

$$I_1 = 1200\ \mathrm{kg\ m^2}, \qquad I_2 = 1400\ \mathrm{kg\ m^2}, \qquad I_3 = 600\ \mathrm{kg\ m^2} \tag{64}$$

with the initial conditions lying in the range $\pi/2 \leq \psi_0 \leq 3\pi/2$ rad, $-225 \leq \Psi_0 \leq 225\ \mathrm{kg\ m^2/sec}$. This case satisfies the linear stability conditions (29). For Case II,

$$I_1 = 1600\ \mathrm{kg\ m^2}, \qquad I_2 = 800\ \mathrm{kg\ m^2}, \qquad I_3 = 1400\ \mathrm{kg\ m^2} \tag{65}$$

with the initial conditions $\pi/2 \leq \psi_0 \leq 3\pi/2$ rad, $-375 \leq \Psi_0 \leq 375\ \mathrm{kg\ m^2/sec}$. This case does not satisfy the linear stability conditions (29).

The remaining initial condition, Θ_0, is determined by solving the energy equation

$$\mathcal{H} = \dot{\psi}_0\Psi_0 + \dot{\theta}_0\Theta_0 + \dot{\phi}_0\Phi_0 - \mathcal{L} + \mathcal{H}_G \tag{66}$$

for Θ_0.

Figures 4 and 5 depict the Poincaré maps for Case I and Case II, respectively. In Fig. 4, there are distinct regions of quasi-periodic motion. This finding corresponds to the reduced phase space, wherein one can observe libration, rotation, and a separatrix connecting the stable and unstable equilibria [9]. In Fig. 4, one can also observe two hyperbolic points. The color in both maps is used to distinguish between short-periodic and long-periodic motion, and is indicative of the time it takes for a given trajectory to cross the section.

In general, the motion of a free rigid body is quasi-periodic, being a superposition of rotation and precession. This corresponds to invariant 2-tori in the phase space. In the present work, it seems as if the presence of the GG torque has not qualitatively changed this behavior. This, however, is not true; since the GG torques are extremely small, it is somewhat difficult to distinguish between the maps shown in Figs. 4 and 5 and the nominal maps of the free-spin case. In order to accentuate the effect of the GG perturbations, we shall examine the *difference* Poincaré maps, which are the maps obtained by subtracting the Poincaré maps of the free-spin case from the maps of the GG-perturbed dynamics.

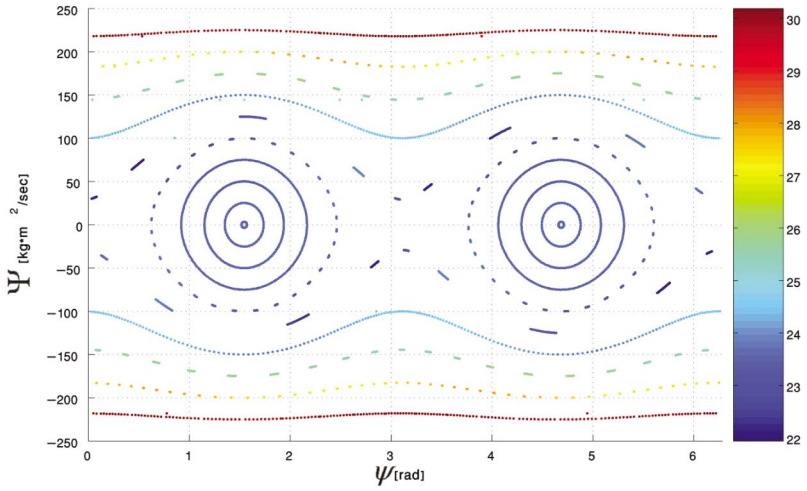

FIG. 4. A Poincaré map for Case I shows region of quasi-periodic motion. Red trajectories on the map indicate long-periodic motion, while blue indicates short-periodic motions. The time units of the color bar are seconds.

Difference Poincaré Maps

To understand the rationale of the difference maps, let $\psi(t)$ and $\tilde{\psi}(t)$ be solutions of the differential equation (60f) for the unperturbed and perturbed cases, respectively. Then, each point on the difference map satisfies

$$\Delta\psi_i = \psi_i - \tilde{\psi}_i \tag{67}$$

In a similar manner, the conjugate momentum difference is

$$\Delta\Psi_i = \Psi_i - \tilde{\Psi}_i \tag{68}$$

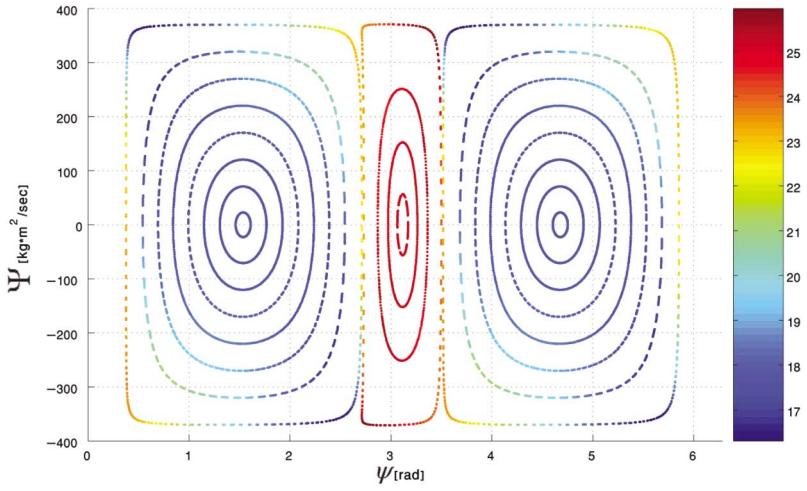

FIG. 5. A Poincaré map for Case II shows regions of quasi-periodic motion and hyperbolic points. Red trajectories on the map indicate long-periodic motion, while blue indicates short-periodic motions. The time units of the color bar are seconds.

and the section cross time difference is

$$\Delta t_i = t_{\Psi_i} - t_{\check{\Psi}_i} \tag{69}$$

Figures 6 and 7 depict the difference maps for Case I and Case II, respectively. Due to the very small magnitude of the perturbation, these maps represent, in fact, the linearized phase space, and can hence be studied from the linear dynamical systems perspective.

Both Figs. 6 and 7 show zero initial differences between the perturbed and unperturbed cases. As the flow evolves, the differences are spirally growing. While the trajectory in Fig. 7 represents a spiral node, the trajectory in Fig. 6 converges onto a limit cycle. This confirms the findings of the linear analysis; Case I is stable and Case II is unstable. Consequently, the spacecraft can be passively stabilized on the collinear point under some constraints on its shape, similarly to the two-body case.

A delicate issue that deserves special attention is the existence of the heteroclinic connection, shown in Fig. 4. This implies that under small periodic perturbations, such as the GG torques, a *heteroclinic* or *horseshoe* chaos may arise [13]. The next section is devoted to studying this issue using the Melnikov integral.

Detecting Chaos by the Melnikov Integral

The small magnitude of the perturbing GG torques allows for the reformulation of the Hamiltonian (32) into

$$\mathcal{H} = \mathcal{H}_0 + \epsilon \mathcal{H}'_G \tag{70}$$

where $\epsilon \ll 1$. Thus, if $x = [\Psi, \Theta, \Phi, \psi, \theta, \phi]^{\mathrm{T}}$, then, based on equations (59), equations (60) can be written as

$$\dot{\mathbf{x}} = \mathbf{f} + \epsilon \mathbf{g} \tag{71}$$

where $\mathbf{f}$ and $\mathbf{g}$ are Hamiltonian vector fields that describe, respectively, the unperturbed motion and the perturbation. When the equations of motion are written in the form of equation (71), the existence of chaos can be determined by using the

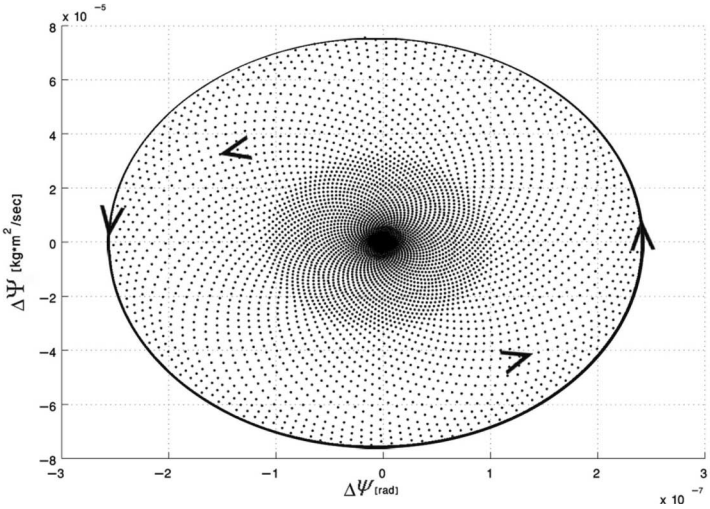

FIG. 6. A difference Poincaré map for Case I shows that the GG-perturbed motion converges onto a stable limit cycle. In this case, passive stabilization is possible.

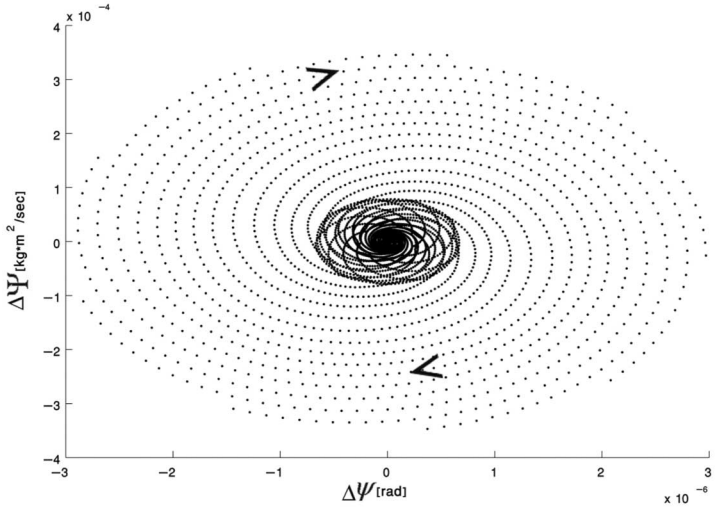

FIG. 7. A difference Poincaré map for Case II shows that the GG-perturbed motion yields a spiral node. In this case, passive stabilization is impossible.

sufficient conditions of the Smale-Birkhoff theorem [26, 27]. According to this theorem, if the manifolds $\mathcal{M}(\mathbf{f})$ and $\mathcal{M}(\mathbf{g})$ generate a diffeomorphism that contains a hyperbolic point, a chaotic behavior will be observed if transverse homoclinic points appear by the manifolds intersections [28, 29].

The Melnikov method [30] provides a simple, analytical test for the existence of chaos in the Smale-Birkhoff sense [28, 21]. This method is commonly used for determining chaos in ubiquitous applications, including quasi-periodically-forced [31, 32, 33] and periodically-excited [13, 34, 35] systems. In Hamiltonian systems such as equations (70)–(71), the Melnikov method can be used to determine if the stable and unstable manifolds intersect transversally by calculating the simple zeros of the *Melnikov integral*

$$M(t_0) = \int_{-\infty}^{\infty} \{\mathcal{H}_0, \mathcal{H}_G\}[\bar{x}(t - t_0), t]\,\mathrm{d}t \tag{72}$$

In equation (72), $\{\,\cdot\,,\,\cdot\,\}$ denotes the Poisson brackets, and $\bar{x}(t)$ is the separatrix. If $M(t_0)$ contains simple zeros, then transverse homoclinic points exist and the system will be chaotic according to the Smale-Birkhoff theorem.

Rendering the Perturbing Hamiltonian Amenable to Melnikov's Method

To utilize the Melnikov method, we must first find an expression for the separatrix, $\bar{x}(t)$ (cf. equation (72)). The separatrix equations are known [11], and were formulated by Elipe [14] in terms of the angular momentum components in the body frame as

$$\bar{g}_1 = H\sqrt{\left(\frac{I_3 - I_2}{I_3 - I_1}\right)\frac{I_1}{I_2}}\,\mathrm{sech}(\nu t) \tag{73a}$$

$$\bar{g}_2 = H\tanh(\nu t) \tag{73b}$$

$$\bar{g}_3 = H\sqrt{\left(\frac{I_2 - I_1}{I_3 - I_1}\right)\frac{I_3}{I_2}}\,\mathrm{sech}(\nu t) \tag{73c}$$

where

$$\nu = \frac{H}{I_2}\sqrt{(I_2 - I_1)(I_3 - I_2)\frac{1}{I_3 I_1}} \tag{74}$$

and H is the magnitude of the angular momentum vector

$$H = \sqrt{g_1^2 + g_2^2 + g_3^2} \tag{75}$$

In order to solve the Melnikov integral (72), all the Poisson brackets with respect to the angular momentum components should be obtained. To that end, we first write an expression for the free-spin Hamiltonian in terms of the angular momentum components [14] as

$$\mathcal{H}_0 = \frac{I_1}{2}g_1^2 + \frac{I_2}{2}g_2^2 + \frac{I_3}{2}g_3^2 \tag{76}$$

The second step is to derive a convenient form of the perturbing Hamiltonian, $\mathcal{H}_G$; that is, we must replace (57) by a form that is amenable to the symbolic calculation of the Melnikov integral. One method of achieving this is to approximate equation (57) by a time-periodic function having the same dominant frequency as the original, periodic, perturbing Hamiltonian. To that end, using equations (57) and (70), we first write

$$\mathcal{H}_G = \epsilon[\beta^2 + \gamma^2 k_2] \tag{77}$$

where

$$\begin{gathered}\epsilon = k_1(k_3 + k_4); \qquad \beta = -c_\psi s_\phi - s_\psi c_\theta c_\phi; \qquad \gamma = s_\phi s_\theta \\ k_1 = \frac{3}{2}(I_2 - I_1); \qquad k_2 = \frac{I_2 - I_1}{I_3 - I_1}; \qquad k_3 = \frac{\mu_1}{r_1^3}; \qquad k_4 = \frac{\mu_2}{r_2^3}\end{gathered} \tag{78}$$

and then attempt to find an approximation of the form

$$\mathcal{H}_G \approx \tilde{\mathcal{H}}_G = \epsilon B_s + \frac{A_m}{k_1}g_3^2\cos(\mu t) \tag{79}$$

where A_m, B_s, and μ are constants to be determined.

Thus, the true and approximated nondimensional perturbing Hamiltonians, respectively, are

$$\mathcal{H}_G' = \frac{\mathcal{H}_G}{\epsilon} = \beta^2 + \gamma^2 k_2 \tag{80}$$

$$\tilde{\mathcal{H}}_G' = \frac{\tilde{\mathcal{H}}_G}{\epsilon} = B_s + \frac{A_m}{\epsilon c_1}g_3^2\cos(\mu t) \tag{81}$$

Figure 8 depicts a comparison between the actual and approximated perturbing Hamiltonians. The time history of the approximating Hamiltonian was plotted with the amplitude $A_m = -2.5 \times 10^{-12}$, frequency $\mu = 5 \times 10^{-7}$ Hz and $B_S = 1$. As can be seen, the approximation captures well the dominant frequency of the true perturbing Hamiltonian, and hence can be safely used for calculating the Melnikov integral.

Solving the Melnikov Integral

After obtaining an approximation for the perturbing Hamiltonian, we can proceed by calculating the Poisson brackets appearing in equation (72) as

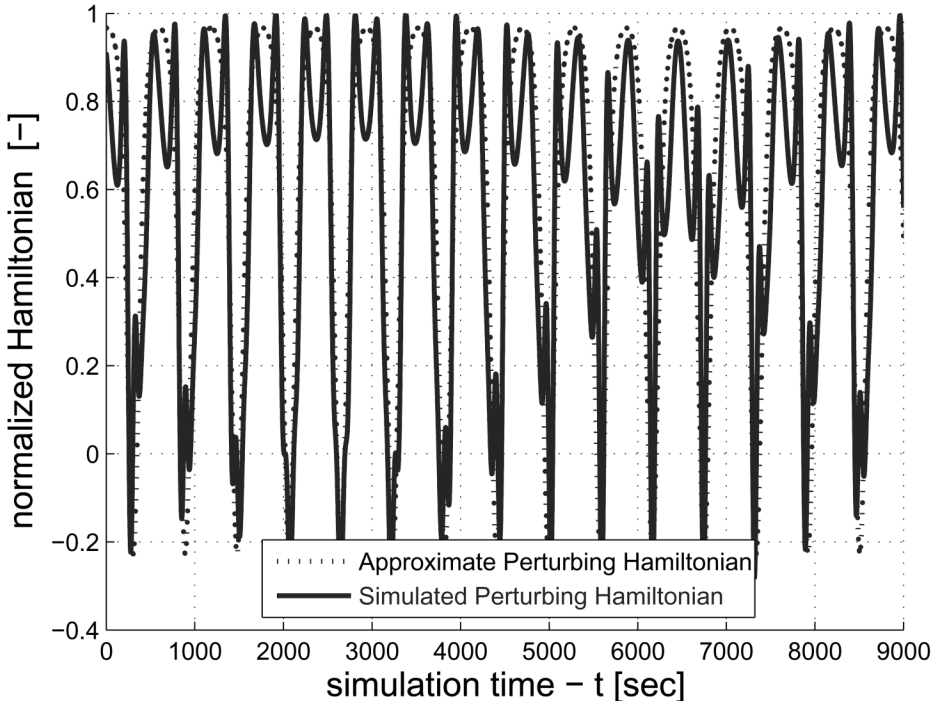

FIG. 8. Comparison Between the Actual Perturbed Hamiltonian and the Analytical Approximation Thereof Shows Good Agreement.

$$\begin{aligned}\{\mathcal{H}_0, \tilde{\mathcal{H}}_G'\} &= \sum_{i=1}^{3}\left(\frac{\partial \mathcal{H}_0}{\partial q_i}\frac{\partial \tilde{\mathcal{H}}_G}{\partial p_i} - \frac{\partial \mathcal{H}_0}{\partial p_i}\frac{\partial \tilde{\mathcal{H}}_G}{\partial q_i}\right)\\ &= \frac{\partial \mathcal{H}_0}{\partial \phi}\frac{\partial \tilde{\mathcal{H}}_G}{\partial \Phi} - \frac{\partial \mathcal{H}_0}{\partial \Phi}\frac{\partial \tilde{\mathcal{H}}_G}{\partial \phi} + \frac{\partial \mathcal{H}_0}{\partial \theta}\frac{\partial \tilde{\mathcal{H}}_G}{\partial \Theta} - \frac{\partial \mathcal{H}_0}{\partial \Theta}\frac{\partial \tilde{\mathcal{H}}_G}{\partial \theta}\\ &\quad + \frac{\partial \mathcal{H}_0}{\partial \psi}\frac{\partial \tilde{\mathcal{H}}_G}{\partial \Psi} - \frac{\partial \mathcal{H}_0}{\partial \Psi}\frac{\partial \tilde{\mathcal{H}}_G}{\partial \psi}\end{aligned} \tag{82}$$

Since $\tilde{\mathcal{H}}_G$ depends on g_3 only, and, according to equations (63c) $\Psi = g_3$, all the terms in equation (82) vanish except for those which directly depend on ψ and its conjugate momentum, Ψ, giving

$$\{\mathcal{H}_0, \tilde{\mathcal{H}}_G\} = \frac{\partial \mathcal{H}_0}{\partial \psi}\frac{\partial \tilde{\mathcal{H}}_G}{\partial \Psi} \tag{83}$$

We can expand equation (83) into

$$\{\mathcal{H}_0, \tilde{\mathcal{H}}_G\} = \left(\frac{\partial \mathcal{H}_0}{\partial g_1}\frac{\partial g_1}{\partial \psi} + \frac{\partial \mathcal{H}_0}{\partial g_2}\frac{\partial g_2}{\partial \psi} + \frac{\partial \mathcal{H}_0}{\partial g_3}\frac{\partial g_3}{\partial \psi}\right)\left(\frac{\partial \tilde{\mathcal{H}}_G}{\partial g_3}\frac{\partial g_3}{\partial \Psi}\right) \tag{84}$$

which simplifies into

$$\{\mathcal{H}_0, \tilde{\mathcal{H}}_G\} = 2\left(\frac{1}{I_1} - \frac{1}{I_2}\right)\frac{A_m}{c_1} g_1 g_2 g_3 \cos(\mu t) \tag{85}$$

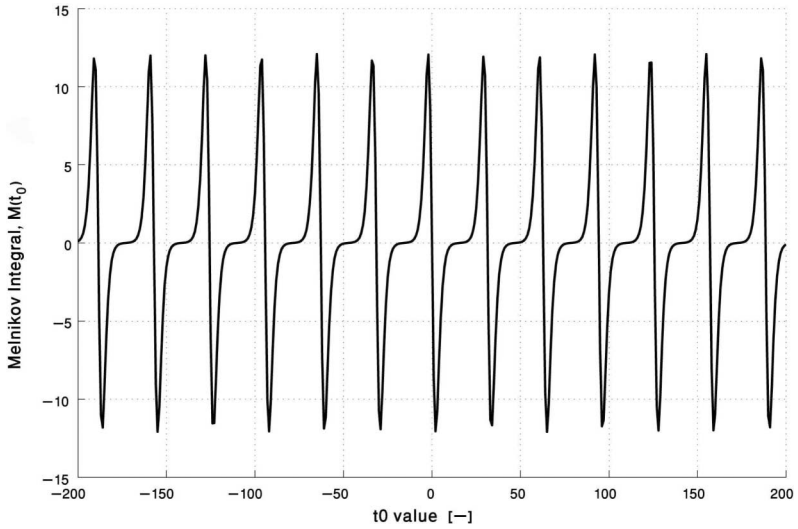

FIG. 9. The Melnikov integral as a function the parameter t_0. The $M(t_0)$-axis crossings are the simple zeros of the Melnikov function.

We can construct the Melnikov integral by substituting (73) and (85) into (72)

$$M(t_0) = 2\left(\frac{I_2 - I_1}{I_2 I_1}\right)\frac{A_m}{c_1} H^3 \int_{-\infty}^{\infty} \sqrt{\left(\frac{I_3 - I_2}{I_3 - I_1}\right)\frac{I_1}{I_2}} \sqrt{\left(\frac{I_2 - I_1}{I_3 - I_1}\right)\frac{I_3}{I_2}} \frac{\tanh[\nu(t - t_0)]}{\cosh^2[\nu(t - t_0)]} \cos(\mu t)\, \mathrm{d}t \tag{86}$$

Rearranging equation (86) yields

$$M(t_0) = 2\nu \frac{I_3}{I_2} A_m H^2 \int_{-\infty}^{\infty} \frac{\tanh[\nu(t - t_0)]}{\cosh^2[\nu(t - t_0)]} \cos(\mu t)\, \mathrm{d}t \tag{87}$$

The integrand appearing in equation (87) is an odd function, and the integral solution equals zero. We can thus conclude that the integral, as a function of t_0, has at least one simple zero. This observation is sufficient to determine that the GG perturbations in the circular RTBP give rise to chaos. To validate this observation, the Melnikov integral may be plotted as a function of t_0. Such a plot is shown in Fig. 9. We can conclude by observing in Fig. 9 that the Melnikov function intersects the $M(t_0) = 0$ line periodically; the intersection points are the simple zeros of $M(t_0)$.

Conclusions

This work studied the effect of gravity gradient (GG) torques in the circular restricted three-body problem (RTBP). It has been found that the total perturbation torque exerted by the two primaries can be considered as a superposition of two separate gravitational torques.

Linearized Euler equations were derived and stability analysis in the Beletskii-DeBra-Delp sense was preformed for the L_2 collinear Lagrange point in the Sun-Earth setup. It has been shown that the Beletskii-DeBra-Delp stability region is smaller in the current problem compared to the two-body problem for the Sun-Earth L_2.

In order to derive the nonlinear equations of motion, a Hamiltonian formalism was adopted. The perturbed Hamiltonian was developed for the circular RTBP assuming that the spacecraft is located at the vicinity of the L_2 point. Due to the complex structure of the dynamics, Poincaré maps were used to quantify the phase space trajectories. Difference Poincaré maps, obtained from subtracting the free-spin maps from the perturbed maps, have validated the results of the linear analysis.

One of the main findings was the analytical proof for the existence of chaos using Melnikov's method. Thus, the dynamics of a spacecraft perturbed by the gravitational torques of two primaries will necessarily exhibit chaos. Using Melnikov's approach was essential since the effect of the GG perturbation is extremely small; hence, alternative approaches such as calculating the Lyapunov exponents or detecting chaotic seas in the Poincaré maps are bound to fail.

Acknowledgments

The authors wish to thank Moshe Guelman and Ilya Ioslovich of the Technion for making valuable suggestions.

References

[1] FARQUHAR, R. W. "The Control and Use of Libration-Point Satellites," Technical Report SUDAAR-350, Stanford University, July, 1968.

[2] FARQUHAR, R. W. "The Utilization of Halo Orbits in Advanced Lunar Operations," Technical Report TN D-6365, NASA, July, 1970.

[3] HÉNON, M. "Vertical Stability of Periodic Orbits in the Restricted Problem," *Astronomy and Astrophysics,* Vol. 28, 1973, pp. 415–426.

[4] RICHARDSON, D. L. "Analytical Construction of Periodic Orbits about the Collinear Points," *Celestial Mechanics,* Vol. 22, 1980, pp. 241–253.

[5] GOMEZ, G. A., MASDEMONT, J., and SIMO, C. "Lissajous Orbits around Halo Orbits," *Advances in the Astronautical Science,* Vol. 95, 1997, pp. 117–134.

[6] HOWELL, K. C. and BARDEN, B. T. "Fundamental Motions near Collinear Libration Points and Their Transitions," *The Journal of the Astronautical Sciences,* Vol. 46, No. 4, 1998, pp. 361–378.

[7] PAPADAKIS, K. E. "The 3D Restricted Three-Body Problem under Angular Velocity Variation," *Astronomy and Astrophysics,* Vol. 425, 2004, pp. 1133–1142.

[8] PERDIOS, E. A. and RAGOS, O. "Asymptotic and Periodic Motion around Collinear Equilibria in Chermnykh's Problem," *Astronomy and Astrophysics,* Vol. 414, 2004, pp. 361–371.

[9] GURFIL, P., ELIPE, A., TANGREN, W., and EFROIMSKY, M. "The Serret-Andoyer Formalism in Rigid-Body Dynamics: I. Symmetries and Perturbations," *Regular and Chaotic Dynamics,* Vol. 12, No. 4, July 2007, pp. 389–425.

[10] COCHRAN, J. E. "Effects of Gravity Gradient Torque on the Rotational Motion of a Triaxial Satellite in a Precessing Elliptic Orbit," *Celestial Mechanics,* Vol. 6, 1972, pp. 127–150.

[11] KINOSHITA, H. "First-Order Perturbations of the Two Finite-Body Problem," *Journal of the Astronautical Society of Japan,* Vol. 24, 1972, pp. 423–457.

[12] ABAD, A., ARRIBAS, M., and ELIPE, A. "On the Attitude of a Spacecraft Near a Lagrangian Point," *Journal of the Astronomical Institute of Czechoslovakia,* Vol. 40, No. 5, 1989, pp. 302–307.

[13] BALAN, R. "Horseshoe and Nonintegrability in the Restricted Case of a Rigid Body in a Central Gravitational Field," Technical Report, Princeton University, June, 1995.

[14] ELIPE, A. "On the Attitude Dynamics of Perturbed Triaxial Rigid Bodies," *Celestial Mechanics and Dynamical Astronomy,* Vol. 81, No. 1–2, 2001, pp. 3–12.

[15] BELETSKII, V. V. "Motion of an Artificial Satellite about its Center of Mass," *Artificial Satellites of Earth,* 1959, pp. 13–31.

[16] DeBRA, D. B. and DELP, R. H. "Rigid Body Attitude Stability and Natural Frequencies in a Circular Orbit," *The Journal of the Astronautical Sciences,* Vol. 8, No. 1, 1961, pp. 14–17.

[17] BROUCKE, R. A. "On the Use of Poincaré Surfaces of Section in Rigid-Body Motion," *The Journal of the Astronautical Sciences,* Vol. 41, 1993, pp. 593–601.

[18] BARKIN, Y. V. "Motion of a Spacecraft about Its Center of Mass at a Libration Point of The Earth-Moon System," *Cosmic Research,* Vol. 18, 1980.
[19] KANE, T. R. and MARSH, E. L. "Attitude Stability of a Symmetric Satellite at the Equilibrium Points in the Restricted Three-Body Problem," *Celestial Mechanics,* Vol. 4, 1971, pp. 78–90.
[20] BLOCH, A. M., GURFIL, P., and LUM, K.-Y. "The Serret-Andoyer Formalism in Rigid-Body Dynamics: II. Geometry, Stabilization and Control," *Regular and Chaotic Dynamics,* to appear.
[21] MARSDEN, J. E. and RATIU, T. S. *Introduction to Mechanics and Symmetry,* Springer, 2004.
[22] KAPLAN, M. H. *Modern Spacecraft Dynamics and Control,* Wiley, 1976.
[23] KANE, T. R. *Spacecraft Dynamics,* Mcgraw-Hill, 1981.
[24] SANDOR, Z., ERDI, B., and FUNK, B. "The Relative Lyapunov Indicators: An Efficient Method of Chaos Detection," *Celestial Mechanical and Dynamical Astronomy,* Vol. 90, 2004, pp. 127–138.
[25] SANDOR, Z., BELLA, R., and TEGER, F. "Short Time Lyapunov Indicators in The Restricted Three-Body Problem," *Celestial Mechanical and Dynamical Astronimy,* Vol. 79, 2001, pp. 29–40.
[26] BIRKHOFF, G. D. *Dynamical Systems,* Vol. RI, A.M.S. Colloquium Publications, Providence, RI, 1927.
[27] SMALE, S. *Diffeomorphisms with Many Periodic Points, Differential and Combinatorial Topology,* Princeton University Press, Princeton, NJ, 1963.
[28] GUCKENHEIMER, J. and HOLMES, P. *Nonlinear Oscillations, Dynamical Systems, and Bifurcations of Vector Fields,* Springer Applied Mathematical Sciences Series, 1983.
[29] WIGGINS, S. *Global Bifurcations and Chaos: Analytical Methods,* Springer Applied Mathematical Sciences Series, 1988.
[30] MELNIKOV, V. K. "On the Stability of the Center for Time Periodic Perturbations," *Transactions of the Moscow Mathematical Sciences Institute,* Vol. 12. MR 156048—Zbl 0135.3100, 1963, pp. 3–52.
[31] MOON, F. C. and HOLMES, W. T. "Double Poincare Sections of a Quasi-Periodically Forced, Chaotic Attractor," *Physics Letters A,* Vol. 111, 1985, pp. 157–160.
[32] WIGGINS, S. "Chaos in the Quasiperiodically Forced Duffing Oscillator," *Physics Letters A,* Vol. 124, 1987, pp. 138–142.
[33] IDE, K. and WIGGINS, S. "The Bifurcation to Homoclinic Tori in the Quasiperiodically Forced Duffing Oscillator," *Physica D,* Vol. 34, 1989, pp. 169–182.
[34] SAHA, L. M., KHAN, A., and SARMA, T. P. "Effects of the Solar Radiation Pressure and Tidal Forces on the Rotational Motion of a Satellite," *Bulletin of the Astronomical Society of India,* Vol. 28, 2000, pp. 147.
[35] STEINDL, A. and TROGER, H. *Chaotic Motion in Mechanical and Engineering Systems,* Springer-Verlag, 1991.